Piezoelectric response and electrical properties of Pb(Zr 1-x Ti x)O 3 thin films: The role of imprint and composition

Thomas W. Cornelius, C. Mocuta, S. Escoubas, A. Merabet, Michael Texier, E.C. Lima, E.B. Araujo, a L Kholkin, Olivier Thomas

Piezoelectric response and electrical properties of $Pb(Zr_{1-x}Ti_x)O_3$ thin films: The role of imprint and composition

T. W. Cornelius, C. Mocuta, S. Escoubas, A. Merabet, M. Texier, E. C. Lima, E. B. Araujo, A. L. Kholkin, and O. Thomas

Citation: Journal of Applied Physics **122**, 164104 (2017);
View online: https://doi.org/10.1063/1.4994939
View Table of Contents: http://aip.scitation.org/toc/jap/122/16
Published by the American Institute of Physics

Piezoelectric response and electrical properties of $Pb(Zr_{1-x}Ti_x)O_3$ thin films: The role of imprint and composition

T. W. Cornelius,[1,a)] C. Mocuta,[2] S. Escoubas,[1] A. Merabet,[1] M. Texier,[1] E. C. Lima,[3] E. B. Araujo,[4] A. L. Kholkin,[5,6] and O. Thomas[1]
[1]*Aix Marseille Univ, Univ Toulon, CNRS, IM2NP Marseille, France*
[2]*Synchrotron SOLEIL, L'Orme des Merisiers, Saint-Aubin-BP 48, 91192 Gif-sur-Yvette Cedex, France*
[3]*Universidade Federal do Tocantins, 77500-000 Porto Nacional, TO, Brazil*
[4]*São Paulo State University (UNESP), School of Natural Sciences and Engineering, Department of Physics and Chemistry, 15385-000 Ilha Solteira, São Paulo, Brazil*
[5]*Department of Physics and CICECO–Aveiro Institute of Materials, University of Aveiro, 3810-193 Aveiro, Portugal*
[6]*ITMO University, St. Petersburg 197101, Russia*

(Received 9 July 2017; accepted 10 October 2017; published online 26 October 2017)

The compositional dependence of the piezoelectric properties of self-polarized $PbZr_{1-x}Ti_xO_3$ (PZT) thin films deposited on $Pt/TiO_2/SiO_2/Si$ substrates ($x = 0.47$, 0.49 and 0.50) was investigated by *in situ* synchrotron X-ray diffraction and electrical measurements. The latter evidenced an imprint effect in the studied PZT films, which is pronounced for films with the composition of $x = 0.50$ and tends to disappear for $x = 0.47$. These findings were confirmed by *in situ* X-ray diffraction along the crystalline [100] and [110] directions of the films with different compositions revealing asymmetric butterfly loops of the piezoelectric strain as a function of the electric field; the asymmetry is more pronounced for the PZT film with a composition of $x = 0.50$, thus indicating a higher built-in electric field. The enhancement of the dielectric permittivity and the effective piezoelectric coefficient at compositions around the morphotropic phase boundary were interpreted in terms of the polarization rotation mechanism and the monoclinic phase in the studied PZT thin films. *Published by AIP Publishing*. https://doi.org/10.1063/1.4994939

INTRODUCTION

The compositional dependence of the structural and electrical properties of $PbZr_{1-x}Ti_xO_3$ (PZT) thin films has been intensively investigated in the past years at compositions around the morphotropic phase boundary (MPB).[1] Both scientific and technological challenges associated with excellent dielectric, ferroelectric, and piezoelectric properties at around the MPB are the main driving forces for the intense research of the PZT system.[2] Various potential applications of PZT thin films were demonstrated including capacitors,[3] micromechanical devices,[4] non-volatile ferroelectric random-access memories,[5] amongst others.

The discovery of a monoclinic phase for some PZT compositions and a consequent redefinition of the composition-temperature phase diagram of the PZT system around the MPB,[6–10] improved the understanding of the high piezoelectric response and other associated properties of this classic ferroelectric material.[11] Despite the progress in PZT ceramics studies, the influence of various factors, such as texture, strain, defects, mechanical coupling between the film and its substrate among others, on the physical properties of PZT thin films as well as the ferroelectrics in general is not yet fully understood. To facilitate the commercialization of the ferroelectric devices based on the sub-micrometer thin films, a deeper understanding of the degradation mechanisms like fatigue[12] and imprint[13] is indispensable. The loss of switchable polarization after repeated polarization reversals characterizes the fatigue in ferroelectric films while asymmetries and electric field shifts in the polarization—electric field (P-E) hysteresis loops symbolize the imprint. While fatigue reduces the lifetime of non-volatile ferroelectric memory devices, the imprint can lead to memory failure through the read or write mechanism. Induced by factors, such as texture, defects, Schottky barriers, and others, the imprint is less understood than the fatigue in ferroelectric films. For this reason, the understanding of the imprint mechanism and its relationship with the physical properties of ferroelectric thin films has motivated investigations on this subject in recent years.

To investigate the physical properties of the ferroelectric thin films, various techniques, such as piezoelectric force microscopy (PFM) and interferometry, are used. Alternatively, *in situ* synchrotron X-ray diffraction combined with the application of an electric field during measurements has been used in recent years to provide useful and precise information beyond the usual applications for structural studies.[14–17] A good review on the time-resolved X-ray diffraction methods can be found in Ref. 18. This *in situ* technique has been used on PZT thin films to study domain switching,[19] the imprint effect,[20,21] as well as the structural evolution during imprint.[22] Although the strain and the piezoelectric properties of ferroelectric thin films have been frequently investigated using interferometry measurements,[23]

a)Author to whom correspondence should be addressed. Present address: IM2NP UMR 7334 CNRS Aix-Marseille Université, Faculté des Sciences, Campus de St Jérôme-Case 262 Avenue Escadrille Normandie Niemen, 13397 Marseille Cedex 20, France.

the use of in *situ* synchrotron X-ray diffraction has demonstrated to be a useful tool for studying the electromechanical response of ferroelectric thin films with appropriate spatial resolution.[24,25]

In the present work, PZT thin films at compositions around the MPB were investigated by piezoelectric force microscopy, electrical measurements, as well as *in situ* synchrotron X-ray diffraction. The P-E hysteresis loops, the measurements of the dielectric permittivity, and the strain as a function of the applied electric field were used to study the compositional dependence of the imprint effect in the thin films.

EXPERIMENTAL

Lead zirconate titanate ($PbZr_{1-x}Ti_xO_3$) thin films with different Ti compositions ($x = 0.47$, 0.49 and 0.50) were deposited by spin coating on $Pt(111)/Ti/SiO_2/Si$ substrates by using a polymeric resin previously prepared by a chemical route based on the Pechini method.[26] The details regarding the film preparation and the used chemical method can be found elsewhere.[10] After the resin deposition, the organics were removed by pyrolysis at 300 °C for 30 min. After a final crystallization in an electric furnace at 700 °C for 1 h, the pyrochlore-free polycrystalline films with no preferential orientation and a thickness of ~700 nm were obtained.

The morphology of the PZT thin films was studied by the transmission electron microscopy using a FEI TITAN microscope operated either at 200 or at 300 kV. For this purpose, the electron transparent lamellas were prepared by focused ion beam (FIB) milling using a double beam FIB microscope (FEI Helios). The surface layer damaged during the milling process was removed using a Fiscione Nanomill apparatus.

Piezoresponse force microscopy (PFM) was performed on the PZT thin films using a modified commercial atomic force microscope (AFM) (Multimode, Nanoscope III, Bruker and Ntegra Prima, NT-MDT). To avoid possible electrostatic effects, N-doped Si tips with a spring constant of 42 N/m were employed in all PFM measurements.

For electrical measurements, a matrix of 10×10 gold electrodes (0.5 mm in diameter each) was deposited by DC sputtering over an area of $1 \times 1\,cm^2$ on the films through a mask to form capacitors. The DC electric field dependence of the dielectric permittivity $\varepsilon(E)$ was measured using an Agilent 4284A LCR meter at 1 kHz. A modified Sawyer-Tower circuit at 20 Hz was used to measure the P-E hysteresis loops.

In situ X-ray diffraction studies were performed at the DiffAbs beamline of SOLEIL Synchrotron (France). The incident monochromatic 10 keV X-ray beam was collimated to a size of $50 \times 50\ \mu m^2$ using a pinhole. This spot size ensured that the footprint of the X-ray beam on the sample surface was always significantly smaller than the size of the top electrodes. This configuration guarantees experiments in the central part of the electrodes where a homogeneous electric field is expected, and the edge effects are avoided. The *in situ* diffraction measurements were performed in coplanar geometry with the sample mounted horizontally on a *xyz* translation-stage for precise lateral sample positioning. The diffracted intensity was monitored using a two-dimensional hybrid pixel area detector (XPAD) with 560×960 pixels and a pixel size of 130 μm,[27] installed at a distance of 650 mm from the sample and covering an angular range of 6° in 2θ direction in a single image. In order to apply an electric field during *in situ* measurements, a selected gold electrode on the top was contacted using a thin wire with a diameter of 150 μm. Then, DC or AC voltages were applied using an Analog Output card (model PXI 3U from ADLINK), allowing the generation of a bipolar tension in the ±10 V range (5 mA maximum current). For AC measurements of hysteresis loops, the X-ray diffraction signal was acquired by accumulating (internally) several thousands of images, each of them with a very short exposure (typically 1 μs) and synchronously taken at the same voltage during the AC cycle. Then, the synchronization was shifted to the next voltage point in order to describe the hysteresis loop.

RESULTS AND DISCUSSION

Figures 1(a), 1(b), and 1(c) summarize the piezoresponse out-of-plane images of the PZT thin films with compositions $x = 0.47$, 0.49, and 0.50, respectively. The white and dark areas in these figures are the signature of the two antiparallel polar states in the studied ferroelectric films, induced by the application of a DC voltage of +30 V (intermediate white square) and −30 V (internal dark square), while the external areas in the images are the characteristic of the piezoresponse of the films before poling. The predominance of the dark contrast over bright contrast in the PFM images before poling indicates that the "negative" domains are predominant over the "positive" domains, suggesting a polarization, which is directed towards the bulk of the film.

The transmission electron microscopy images of PZT thin films with compositions of $x = 0.47$ and $x = 0.49$ are presented in Figs. 1(d) and 1(e), respectively. The stacking formed by the various layers (SiO_2, Ti, Pt, PZT, and Au) can be easily distinguished. The ferroelectric layers in both figures show a nano-granular microstructure with grain size ranging from 70 to 130 nm. The thickness of the two films amounts to 800 ± 50 and 550 ± 50 nm for $x = 0.47$ and $x = 0.49$, respectively. No preferential crystalline orientation is evidenced.

Figure 2(a) shows the DC electric field dependence of dielectric permittivity $\varepsilon(E)$ at 1 kHz for PZT films with different compositions. For zero DC electric field, the measured values for the dielectric permittivity were $\varepsilon = 461$, 390 and 263 for films with compositions of $x = 0.47$, 0.49, and 0.50, respectively. These values are slightly smaller than the previous dielectric measurements performed at the same PZT films compositions,[28] which demonstrated a maximum dielectric permittivity at $x = 0.48$. The higher dielectric permittivity observed for the composition $x = 0.47$ in the present work agrees with several reports in the literature for PZT thin films,[29] which demonstrated a ε maximum close to MPB ($x \sim 0.48$). Around the MPB, the dielectric permittivity ε_{33} monotonously increases along the [001] direction in the rhombohedral side and along [111] in the tetragonal side as the spontaneous polarization direction increases, as predicted

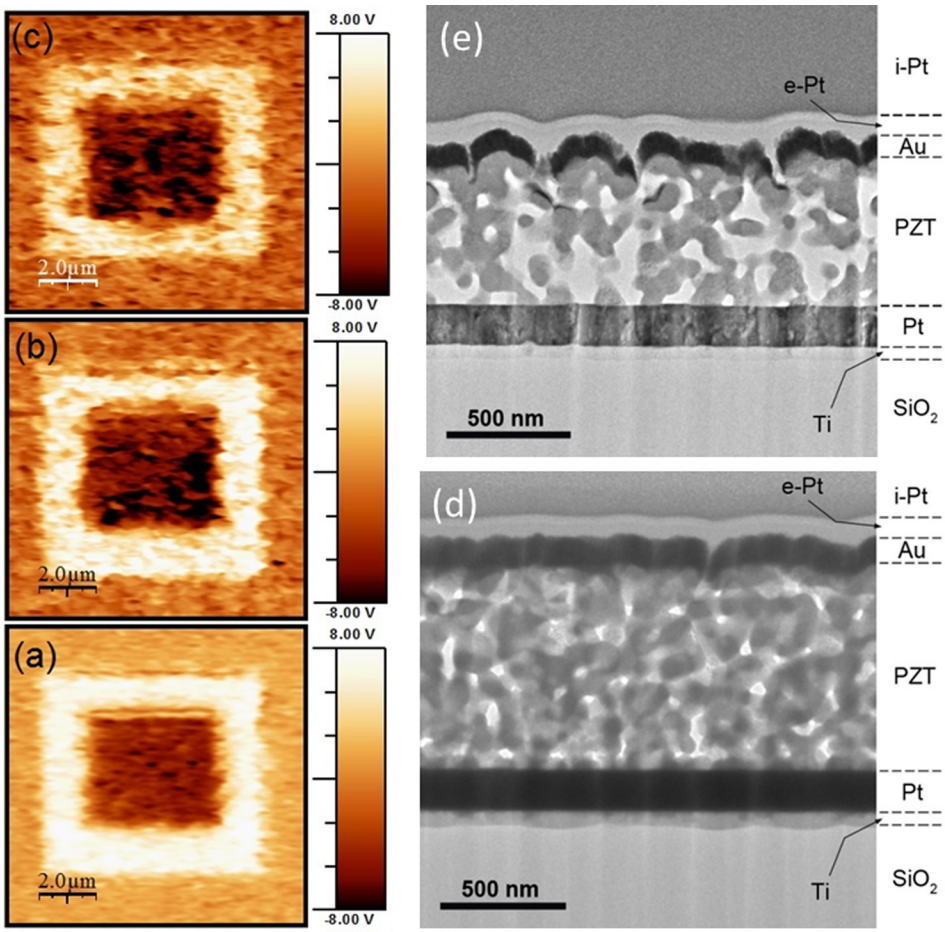

FIG. 1. PFM out-of-plane images (10×10 μm^2) of PZT thin films with Ti concentration x of (a) 0.47, (b) 0.49, and (c) 0.50. Transmission electron micrograph images of PZT thin films with compositions (d) $x = 0.47$ and (e) $x = 0.49$. The Pt protective layers deposited, using electron and ion beams during the TEM sample preparation process, are labelled e-Pt and i-Pt, respectively.

by phenomenological approach.[30] The maximal ε reported has an intrinsic correlation with the piezoelectric response associated with a monoclinic phase in the PZT system, as will be discussed in the following.

The asymmetries observed in the $\varepsilon(E)$ curves in Fig. 2(a) suggest the presence of a built-in electric field in the ferroelectric thin films. Considering that for ferroelectrics the maximum in the $\varepsilon(E)$ curves is associated with the double coercive field,[31] the asymmetry in the coercive field is estimated by the difference $\Delta E_c = E_c^+ - E_c^-$. This estimation results in $\Delta E_c = 0.7$, 1.5, and 11.3 kV/cm for concentrations of 47, 49, and 50%Ti, respectively, suggesting an imprint effect that is more pronounced for the film with 50%Ti and tends to disappear for the film with 47%Ti.

The P–E hysteresis loops of the PZT films with different Ti concentrations displayed in Fig. 2(b) show high saturation (P_s) and remanent (P_r) polarization for $x = 0.47$, which is in agreement with several reports in the literature. A closer examination of the hysteresis data reveals asymmetries with clear shifts in the electric fields that are highlighted by the inset in Fig. 2(b) showing $\Delta E_c = E_c^+ - E_c^-$ as a function of the Ti concentration. While ΔE_c is zero for $x = 0.47$ it increases with the increasing Ti concentration reaching 19.7 kV/cm for $x = 0.50$. Both the asymmetry and the shifts in the P–E hysteresis loops and $\varepsilon(E)$ curves evidence an imprint effect in the PZT films under study. The shift towards positive electric fields ($\Delta E_c > 0$) suggests the presence of a built-in electric field pointing towards the film-substrate interface. Similar imprint effects were also observed for thicker PZT films prepared by sol-gel methods.[32] Although the previous analyses on these PZT films[33] with different thicknesses have excluded Schottky barriers and/or mechanical coupling near the film-substrate interface as the main mechanisms responsible for the imprint effect, the origin of the imprint in these films is still under discussion.

As demonstrated before, the PZT thin films under investigation are nanogranular with a high porosity. While other experimental techniques may generally measure lower piezoelectric coefficients for such nanoporous samples since the methods rely on the dilatation of the sample as a whole, X-ray diffraction techniques determine the dilatation of the atomic lattice, which is independent of the thin film morphology. Moreover, various crystallographic directions/planes can be accessed on the same polycrystalline sample, by performing the diffraction measurement at corresponding different Bragg peaks. Thus, they are pre-destined techniques to study piezoelectricity in nanocrystalline and nanoporous specimens. Synchrotron X-ray diffraction patterns of the PZT thin films with different compositions (including the top and bottom electrodes) are shown in Fig. 3. The diffractograms were recorded with a fixed incident angle of 10° to suppress (or at least largely reduce) the signals of the Si substrate, the Pt bottom electrode, and the Au top electrode. The indexed 100 and 110 peaks with a maximum at around $2\theta = 17.6°$ and 24.9° are associated with the tetragonal phase (P4 mm space group) of the PZT, while the peaks at

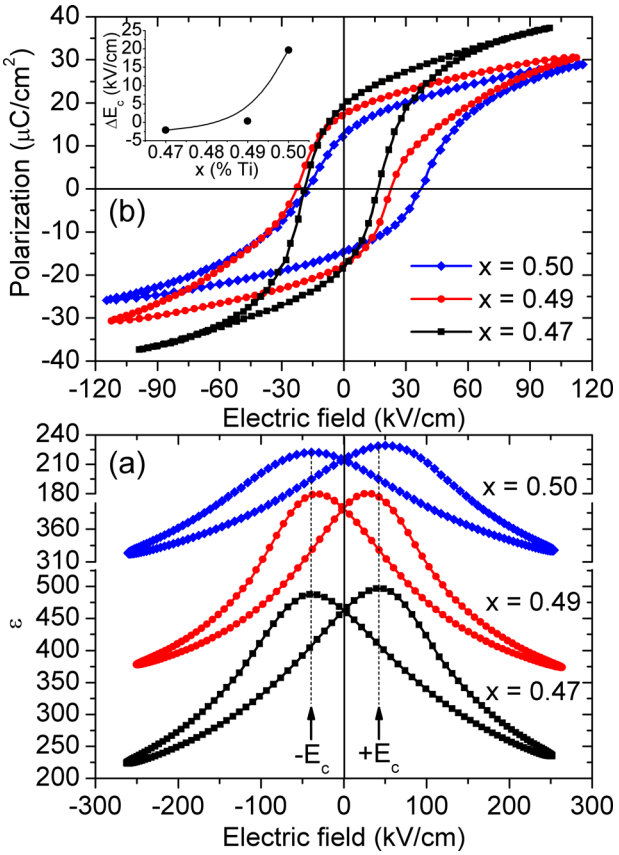

FIG. 2. (a) Dependence of the dielectric permittivity on electric field $\varepsilon(E)$ recorded at 1 kHz and (b) *P-E* hysteresis loops recorded at 20 Hz of PZT thin films for the compositions x = 0.47, 0.49, and 0.50. The inset in panel (a) shows the composition dependence of $\Delta E_c = E_c^+ - E_c^-$ from *P-E* hysteresis loops.

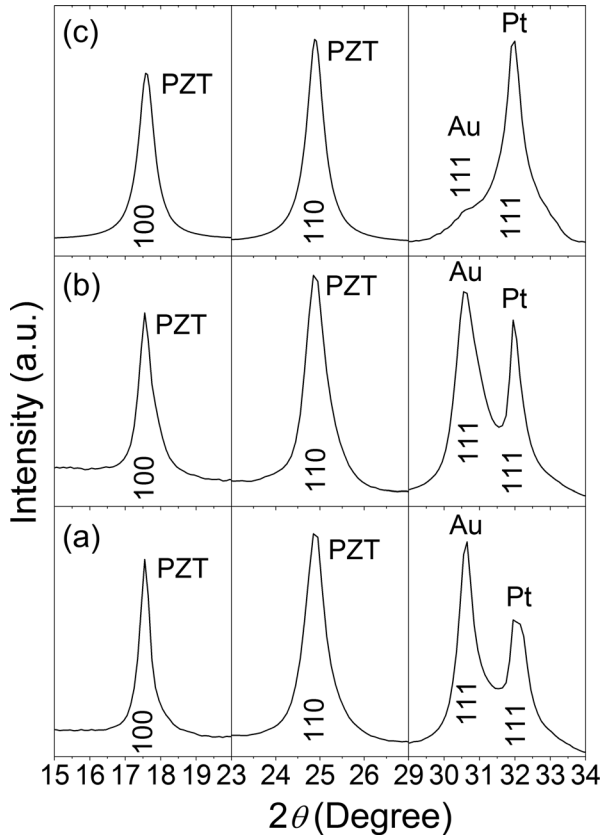

FIG. 3. X-ray diffraction patterns of PZT thin films with Ti concentrations *x* of (a) 0.47, (b) 0.49, and (c) 0.50.

$2\theta = 30.6°$ and 32.0° are attributed to the gold top electrode and to the platinum bottom electrode, respectively.

From the width of the PZT Bragg peaks, the mean size of the ordered domains (crystallite size) was calculated using the Scherrer equation $\tau = (K\lambda)/(\beta \cos\theta)$,[34] where τ is the mean size of the crystallite size, K is a dimensionless shape factor, λ is the X-ray wavelength, and β is the line broadening at half the maximum intensity (FWHM). The wavelength $\lambda = 1.240$ Å refers to the X-ray beam energy $E = 10$ keV while the β line broadening was obtained from fitting Bragg peaks using a Lorentzian. Considering the instrumental resolution ~0.02° and the detector resolution ~0.01°, the average coherent diffracting domain size is τ ~26 nm. This value is 2–3 times smaller than the one reported by the TEM findings on these samples, but remains coherent with the sub-structure of the grains sometimes visible in the TEM micrographs.

For *in situ* X-ray diffraction, an electric field was applied by electrically contacting a selected top gold electrode with a thin wire and applying a voltage U ranging from –10 to +10 V. First, the static measurements were realized by changing U in pre-defined steps (typically 1 V) and recording the diffraction signal for a pre-selected Bragg peak. At each voltage step, a 2D diffraction pattern was recorded with an exposure time of 10 s. The diffraction patterns show a segment of the Debye-Scherrer ring (see supplementary material). Before image analysis, geometrical corrections were applied on the curved signal stemming from the powder ring transforming the pixel coordinates of the detector into angular ones (2θ and azimuth). The 2θ Bragg peak profile was extracted following an azimuthal regrouping of the data. From the displacement of the Bragg peak position when applying a voltage (electric field), the piezoelectric strain induced in the PZT film was deduced.

Figure 4(a) shows the piezoelectric strain as a function of the applied electric field for the 110 peak of the PZT thin film at x = 0.47 (PZT47) during 5 voltage cycles. The "butterfly loops" shown in this figure are caused by the piezoelectric hysteresis in the film. Taking the initial position of the Bragg peak for the non-polarized thin film recorded at $U = 0$ V as reference, the butterfly loops exhibit solely positive strain values. The fact that the hysteresis curves never return to the original point indicates that the films are polarized during each cycle similar to the *P-E* hysteresis loops. Moreover, with the increasing number of cycles the butterfly loops become more pronounced (or smoother), the peak-to-peak value increases, and the loops shift to more positive strain values (by about 0.01% for the 5th cycle with respect to the first one). The butterfly loops for all cycles are almost symmetric indicating a negligible built-in electric field.

Figure 4(b) shows the electric field dependence of the piezoelectric strain for the 100 and the 110 peaks of the PZT thin film for the x = 0.47 composition. For comparison, the strain induced in the 111 peak of the Pt bottom electrode is also included as a reference. While both 100 and 110 peaks describe clearly the "butterfly loops," a typical response of a ferroelectric material, the 111 Pt peak is not affected by the

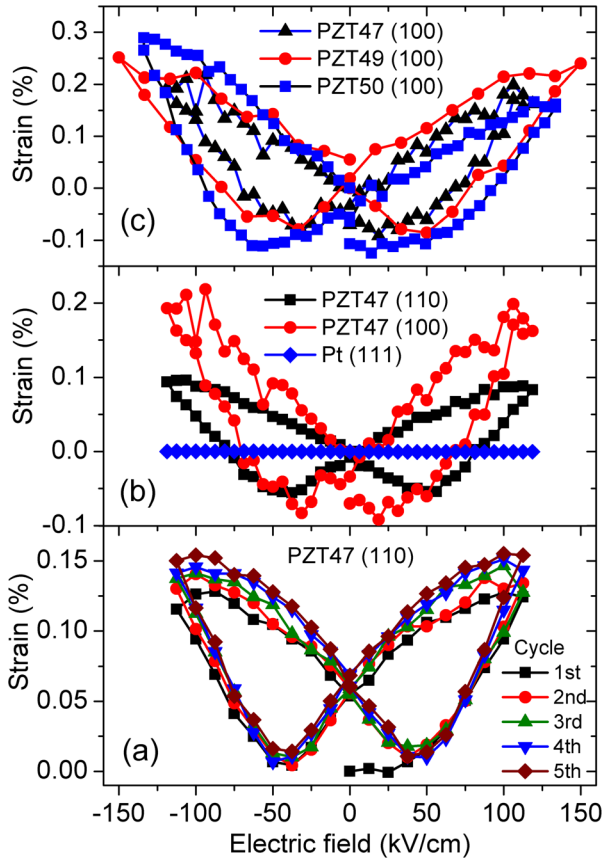

FIG. 4. (a) Piezoelectric strain induced in a PZT thin film with x = 0.47 (PZT47) measured on the PZT 110 Bragg peak for 5 consecutive voltage cycles. (b) Butterfly loops of different PZT Bragg peaks for PZT thin films with composition x = 0.47 (PZT47). The Pt 111 Bragg peak is also measured as reference. (c) Piezoelectric strain induced along the PZT [100] direction for PZT thin films with different Ti concentrations x of 0.47 (PZT47), 0.49 (PZT49), and 0.50 (PZT50).

applied voltage, as expected, since platinum is not piezoelectric. It is further observed that the induced piezoelectric strain is larger along the PZT [100] direction than for the [110] direction. Consequently, the piezoelectric coefficient is higher along the [100] than along the [110] direction in the PZT thin film with $x = 0.47$.

The electric field dependence of the piezoelectric strain along the [100] direction for PZT thin films of different compositions is shown in Fig. 4(c). While the butterfly loops of the PZT films with composition 0.49 are almost symmetric, a pronounced asymmetry is apparent for the composition x = 0.47 and x = 0.50. Again, the asymmetries of the butterfly loops confirm an imprint effect and reflect the built-in electric field in the studied PZT films, as discussed earlier and evidenced by P-E hysteresis loops and $\varepsilon(E)$ curves shown in Fig. 2. Based on the butterfly curves in Fig. 4(c) and considering $d_{33} = (\partial S_3/\partial E_3)_T$ where S_3 is the strain and E_3 is the electric field along the same c-direction, the effective piezoelectric coefficient $d_{33,\mathrm{eff}}$ was determined for different compositions at the same electric field $E = \pm 119$ kV/cm. This effective $d_{33,\mathrm{eff}}$ quantity is, in fact, a good approximation of d_{33} (along the film normal): with an incident angle of 10° and Bragg angles of 18° or 25°, respectively; the scattering vector is rather close (within 5°) to the film normal.

For the positive electric field ($E = +119$ kV/cm) in Fig. 4(c), the calculated effective piezoelectric coefficients along the [100] direction were 137, 180, and 140 pm/V for the PZT compositions x = 0.47, 0.49, and 0.50, respectively, while for the negative electric field ($E = -119$ kV/cm), the calculated effective coefficient were, respectively, 164, 189, and 223 pm/V. For all the studied compositions, the $d_{33,eff}$ coefficients were higher for the negative than for the positive electric field. The asymmetries $\Delta d_{33,eff} = d^{-}_{33,eff} - d^{+}_{33,eff}$ were quantified to 27, 9, and 93 pm/V for the compositions $x = 0.47$, 0.49, and 0.50, respectively. These results agree with those obtained from P-E hysteresis loops, which also demonstrate the highest asymmetry in the coercive field ΔE_c for the composition $x = 0.50$. Consequently, the higher asymmetry observed in Δd_{33} at $x = 0.50$ indicates that the imprint effect is more pronounced at this PZT composition than for films with $x = 0.47$ and 0.49. The lowest $\Delta d_{33,eff}$ illustrates that the PZT film at the composition $x = 0.47$ is almost imprint free and, as a consequence, the observed $d_{33,eff}$ ~180 pm/V in the present work is a "true" value, which is in excellent agreement with the effective coefficients measured by a double beam laser interferometer method for PZT films prepared by the sol-gel technique.[20] The existence of point defects such as complex vacancies and Ti^{3+} centers are the most probable origin for the imprint effect observed in these PZT films at different compositions.[10]

The origin of the high piezoelectric response reported in the PZT system at compositions around the MPB (x ~0.48) has been interpreted in terms of the polarization rotation via an intermediate monoclinic phase between the rhombohedral and the tetragonal phases in the phase diagram of the PZT system.[35] Based on the elongation of the polar vector in ferroelectrics with no monoclinic phases, the polarization extension has been used to understand the electromechanical properties enhancement in these systems in terms of a more general mechanism.[36] On the other hand, the structural stabilities responsible for large piezoelectric and dielectric properties was comprehensively considered as only part of the problem and, alternatively, it has also been proposed that both polarization rotation and polarization mechanisms can be used to interpret the enhanced electromechanical properties in solid solutions with MPB.[37] However, the evidences that the piezoelectric strain is not along the polar directions but along the directions associated with the monoclinic distortion leads us to suppose that the polarization rotation is predominantly the mechanism responsible for large piezoelectric response in the PZT system with compositions around the MPB.[26]

The stability of the monoclinic phase in the PZT system has been reproduced from first-principles calculations[38] such as the drastic increasing in $d_{33,eff}$ early predicted from phenomenological calculations[21] for rhombohedral phase of the PZT along the [001] direction could be understood. The stability of this intermediate monoclinic phase of space group Cm in the PZT was also explained using higher-order Devonshire theory to conclude that the polarization vector $\vec{P}$ rotate into the $(11\bar{0})$ mirror plane continuously from the tetragonal side but discontinuously from the rhombohedral side.[39] Although this effect will largely cancel in a randomly

oriented ceramic, the polarization rotation mechanism explains the maximum dielectric permittivity and effective piezoelectric coefficient observed at a composition of around $x = 0.48$ in randomly oriented PZT thin films.[20] Despite the imprint effect on the effective piezoelectric coefficient along the [100], the $d_{33,eff}$ coefficient values in the present work are in very good agreement with other reports in the literature.[20] Unfortunately, *in situ* synchrotron, the X-ray diffraction measurements were not made on the PZT film with composition $x = 0.48$ to give us additional information about the imprint effect on the $d_{33,eff}$ coefficient between $x = 0.47$ and 0.49.

Besides the DC measurements described earlier, AC (unipolar and bipolar) experiments were performed applying alternating electric field with frequencies ranging from 60 Hz to 31 kHz. Figure 5(a) shows the strain induced during bipolar electric field cycles at 3.125 kHz frequency for (110) peaks of PZT films with compositions $x = 0.47$ and 0.49, while the piezoelectric response of these films is shown in Fig. 5(b) for both 100 and 110 peaks for unipolar electric field with the same applied frequency. The inset in Fig. 5(b) shows the strain dependence of the 110 peak of the PZT film with $x = 0.47$ for electric fields with different frequencies. Within the experimental uncertainties, the piezoelectric response along the [110] direction is not affected by the frequency within the range studied. The strain induced along the [110] direction is essentially the same for the two different films, while along the [100] direction the piezoelectric strain is higher for $x = 0.49$. However, the strain induced by AC electric fields is smaller than for static electric fields. The lower piezoelectric strain for AC electric fields compared to DC fields cannot be assigned to domain switching since already for frequencies of 62 Hz, which are far below any domain switching frequencies, the piezoelectric response is reduced. In addition, for higher frequencies of up 31 kHz no changes in the piezoelectric coefficient are observed. Thus, the diminishing of the piezoelectric effect for AC fields has to be caused by an additional phenomenon associated with the porous nature of the studied PZT thin films. Further studies are needed to better understand the porous effects on these piezoelectric properties of ferroelectric thin films.

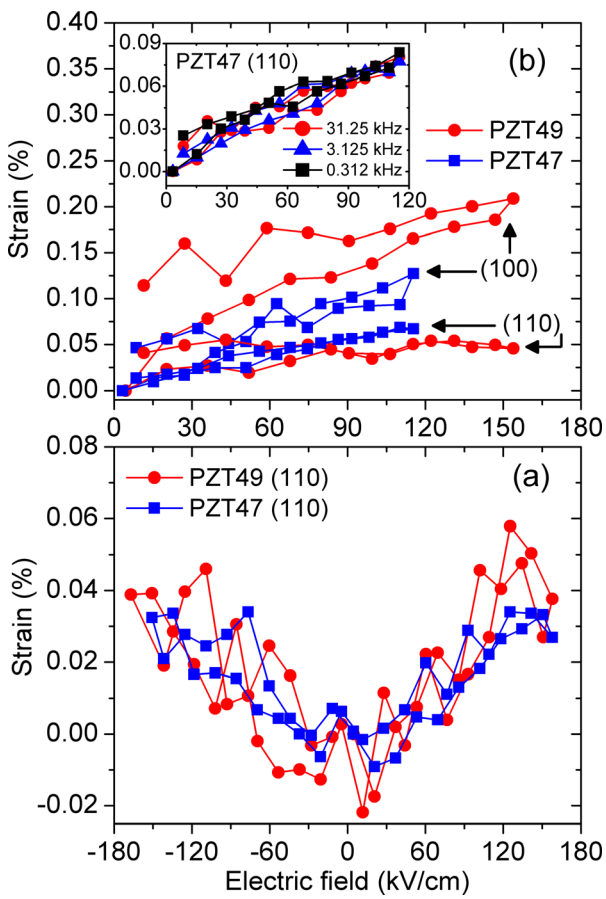

FIG. 5. Piezoelectric strain as a function of (a) bipolar and (b) unipolar electric fields with an AC frequency of 3.125 kHz for films of different compositions (x = 0.47 and 0.49). The inset of (b) shows the piezoelectric strain along the PZT [110] direction as a function of unipolar electric fields with different AC frequencies for the PZT47 thin film.

In the paper of Guo *et al.*,[26] the changes in the unit cell induced by an electric field using high-resolution synchrotron X-ray diffraction revealed the origin of the high piezoelectric response of PZT ceramics. For poled PZT ceramics with tetragonal composition, the observed decrease in the 200 and 220 intensities followed by an increase in the 002 and 202 intensities with respect to the unpoled samples were due to the changes in the domain population. These changes in the domain population could also be observed in the rhombohedral $(111)/(11\bar{1})$ and $(220)/(2\bar{2}0)$ intensity ratios. In addition, no shift observed in the rhombohedral 111 or tetragonal 001 peak positions confirms that the elongation does not occur along the polar directions after the electric field application, but along the directions associated with the monoclinic phase.[26]

On the effects of the electric field on our PZT films, we observed for x = 0.47 composition that the rhombohedral 110 peak position shifted to lower 2θ angle after the application of an electric field of 150 kV/cm (not shown here), while the peak intensity decreased. The peak position shifting to lower 2θ is essentially the same observed for rhombohedral and tetragonal PZT ceramics after poling, whereas the decrease observed in the rhombohedral 110 peak indicates changes in the domain population. However, it cannot confirm if these changes are associated with the monoclinic phase in the studied PZT film. Most of these difficulties are associated with the larger width of diffraction peaks of thin films compared with bulk ceramics due to smaller grain size. However, an adequate deconvolution of the peaks by using Rietveld refinements may give an indicative of the coexistence between the monoclinic-tetragonal and monoclinic-rhombohedral for PZT thin films with compositions around the MPB.[19] Therefore, the decreasing rhombohedral 110 peak intensity after poling is caused by a domain population increase along the monoclinic plane of the studied PZT thin film.

CONCLUSIONS

In summary, the composition dependence around MPB of the electrical properties and of the piezoelectric strain investigated by *in situ* synchrotron X-ray diffraction was

studied in the present work. Piezoelectric strain recorded along the crystalline [100] and [110] directions of the films with different compositions reveal asymmetrical butterfly loops, which is a clear evidence of an imprint effect observed in the studied PZT thin films. The dielectric permittivity and $d_{33,eff}$ effective piezoelectric coefficient enhancement around the MPB were interpreted in terms of the polarization rotation mechanism and the monoclinic phase in randomly oriented PZT thin films. Asymmetries on butterfly curves indicate that the effective coefficients were higher for negative than positive electric field and that these asymmetries were more pronounced in the PZT film with composition $x = 0.50$. This result agrees with the highest asymmetry ΔE_c observed in the coercive electric field of the P-E hysteresis loops and $\varepsilon(E)$ curves. These results suggest that the imprint effect is more pronounced for the film with $x = 0.50$ and tends to disappear for the film with $x = 0.47$.

SUPPLEMENTARY MATERIAL

See supplementary material for raw 2D detector images and the illustration of the applied geometrical corrections on the curved signal stemming from the powder ring, thus transforming the pixel coordinates of the detector into angular ones (2θ and azimuth) from which the 2θ Bragg peak profile was extracted.

ACKNOWLEDGMENTS

The authors gratefully acknowledge the SOLEIL Synchrotron for allocating beam time. Detector and Electronics Support Groups, as well as P. Joly, are acknowledged for the excellent technical support during the experimental campaign at SOLEIL Synchrotron on DiffAbs beamline. We would like to express our gratitude to the CAPES-COFECUB (Project No. 801-14), CNPq (Grant No. 304604/2015-1 and Project No. 400677/2014-8) and FAPESP (Project No. 2010/16504-0) for their financial support. A.K. acknowledges CICECO-Aveiro Institute of Materials (Ref. FCT UID/CTM/50011/2013) financed by the national funds through the FCT/MEC and, when applicable, cofinanced by FEDER under the PT2020 Partnership Agreement. This work was in part supported by the Government of Russian Federation (Grant No. 074-U01).

[1]H. D. Chen, K. R. Udayakumar, C. J. Gaskey, and L. E. Cross, Appl. Phys. Lett. **67**, 3411 (1995).
[2]B. Jaffe, W. R. Cook, and H. Jaffe, *Piezoelectric Ceramics* (Academic, New York, 1971), p. 146.
[3]M. Miyake, J. F. Scott, X. J. Lou, F. D. Morrison, T. Nonaka, S. Motoyama, T. Tatsuta, and O. Tsuji, J. Appl. Phys. **104**, 064112 (2008).
[4]C. H. Ahn, K. M. Rabe, and J. M. Triscone, "Ferroelectricity at the nanoscale: Local polarization in oxide thin films and heterostructures," Science **303**, 488–491 (2004).
[5]J. F. Scott and C. A. P. de Araujo, Science **246**, 1400 (1989).
[6]B. Noheda, D. E. Cox, G. Shirane, J. A. Gonzalo, L. E. Cross, and S.-E. Park, Appl. Phys. Lett. **74**, 2059 (1999).
[7]B. Noheda, J. A. Gonzalo, L. E. Cross, R. Guo, S. E. Park, D. E. Cox, and G. Shirane, Phys. Rev. B **61**, 8687 (2000).
[8]N. Zhang, H. Yokota, A. M. Glazer, and P. A. Thomas, Acta Crstallogr. B **67**, 386–398 (2011).
[9]N. Zhang, H. Yokota, A. M. Glazer, Z. Ren, D. A. Keen, D. S. Keeble, P. A. Thomas, and Z.-G. Ye, Nat. Commun. **5**, 5231 (2014).
[10]S. Gorfman, D. S. Keeble, A. M. Glazer, X. Long, Y. Xie, Z.-G. Ye, S. Collins, and P. A. Thomas, Phys Rev. B **84**, 020102(R) (2011).
[11]B. Noheda and D. E. Cox, Phase Trans. **79**, 5 (2006).
[12]H. Zhu, Y. Chen, D. Chu, S. Feng, Y. Zhang, and P. Wang, Jpn. J. Appl. Phys., Part 1 **55**, 091501 (2016).
[13]E. B. Araujo, E. C. Lima, I. K. Bdikin, and A. L. Kholkin, Ferroelectrics **498**, 18 (2016).
[14]J. Young, P. Chen, R. J. Sichel, S. J. Callori, J. Sinsheimer, E. M. Dufresne, M. Dawber, and P. G. Evans, Phys. Rev. Lett. **107**, 055501 (2011).
[15]S. Gorfman, H. Simons, T. Iamsasri, S. Prasertpalichat, D. P. Cann, H. Choe, U. Pietsch, Y. Watter, and J. L. Jones, Sci. Rep. **6**, 20829 (2016).
[16]A. Pramanick, D. Damjanovic, J. E. Daniels, J. C. Nino, and J. L. Jones, J. Am. Ceram. Soc. **94**, 293–309 (2011).
[17]S. Gorfman, O. Schmidt, V. Tsirelson, M. Ziolkowski, and U. Pietsch, Z. Anorg. Allg. Chem. **639**, 1953–1962 (2013).
[18]S. Gorfman, Crystallogr. Rev. **20**, 210–232 (2014).
[19]K. S. Lee, Y. K. Kim, S. Baik, J. Kim, and I. S. Jung, Appl. Phys. Lett. **79**, 2444 (2001).
[20]I. Baturin, N. Menou, V. Shur, C. Muller, D. Kuznetsov, J. L. Hodeau, and A. Sternberg, Mater. Sci. Eng. B **120**, 141–145 (2005).
[21]T. Iamsasri, G. Esteves, H. Choe, M. Vogt, S. Prasertpalichat, D. P. Cann, S. Gorfman, and J. L. Jones, J. Appl. Phys. **122**, 064104 (2017).
[22]J. L. Cao, K. Zhang, A. Solbach, Z. Yue, H. H. Wang, Y. Chen, and U. Klemradt, Mater. Sci. Forum **687**, 292–296 (2011).
[23]A. L. Kholkin, Ch. Wütchrich, D. V. Taylor, and N. Setter, Rev. Sci. Instrum. **67**, 1935 (1996).
[24]M. C. Ehmke, J. Glaum, M. Hoffman, J. E. Blendell, and K. J. Bowman, J. Am. Ceram. Soc. **96**, 2913 (2013).
[25]A. Davydok, T. W. Cornelius, C. Mocuta, E. C. Lima, E. B. Araùjo, and O. Thomas, Thin Solid Films **603**, 29–33 (2016).
[26]M. Kakihana, J. Sol-Gel Sci. Technol. **6**, 7 (1996).
[27]C. Mocuta, M.-I. Richard, J. Fouet, S. Stanescu, A. Barbier, C. Guichet, O. Thomas, S. Hustache, A. Zozulya, and D. Thiaudière, J. Appl. Cryst. **46**, 1842 (2013).
[28]E. B. Araújo, E. C. Lima, I. K. Bidkin, and A. L. Kholkin, Adv. Mater. Res. **975**, 9 (2014).
[29]H. D. Chen, K. R. Udayakumar, C. J. Gaskey, and L. E. Cross, Appl. Phys. Lett. **67**, 3411 (1995).
[30]X. H. Du, J. Zheng, U. Belegundu, and K. Uchino, Appl. Phys. Lett. **72**, 2421 (1998).
[31]H. Li and G. Subramanyam, IEEE Trans. Ultrason. Ferroelectr. Freq. Control **56**(9), 1861 (2009).
[32]B. Wang, K. W. Kwok, H. L. W. Chan, and C. L. Choy, Appl. Phys. A **79**, 643–646 (2004).
[33]E. B. Araújo, E. C. Lima, I. K. Bidkin, and A. L. Kholkin, J. Appl. Phys. **113**, 187206 (2013).
[34]A. Patterson, Phys. Rev. **56**, 978 (1939).
[35]R. Guo, L. E. Cross, S. E. Park, B. Noheda, D. E. Cox, and G. Shirane, Phys. Rev. Lett. **84**, 5423 (2000).
[36]D. Damjanovic, IEEE Trans. Ultrason. Ferroelectr. Freq. Control **56**, 1574 (2009).
[37]D. Damjanovic, Appl. Phys. Lett. **97**, 062906 (2010).
[38]L. Bellaiche, A. Garcia, and D. Vanderbilt, Phys. Rev. Lett. **84**, 5427 (2000).
[39]D. Vanderbilt and M. H. Cohen, Phys. Rev. B **63**, 094108 (2001).